Understanding Thin Cambered Airfoils and their Solar Aircraft Applications

Galen J. Suppes* and Adam B. Suppes†

Homeland Technologies, LLC, Charlottesville, VA 22911

Modified thin cambered solar panels may be used as wing sections, thereby enabling high solar panel productivity in ultralight designs to directly displace battery and fuel costs. Computational studies were performed to better understand limits in performance and how to achieve high lift-drag ratios (*L/D*). Induced thrust at leading sections of thin cambered airfoils are key to creating high *L/D* in 2D airfoils; however, the dynamics significantly change when loss of lift pressures across side edges of low aspect ratio (*AR*) designs diminish the propagation of trailing-section lift-generating sources forward. Preliminary studies on use of fences, distributed propulsion, and novel airframe designs were investigated to overcome these challenges of using thin cambered wings. Wing designs previously dismissed as having inadequate lift coefficients are now prime candidates for solar aircraft where bifacial solar modules can be greater than 2X the productivity of solar panels on Earth's surface.

Nomenclature

2D	=	two dimensional.
3D	=	three Dimensional
AoA	=	air's angle of attack (°)
AR	=	aspect ratio, defined as the span divided by a representative longitudinal chord length

* Chief Engineer, Homeland Technologies, LLC, gjsuppes@gmail.com
† Senior Research Engineer, Homeland Technologies, LLC

Camber = curvature of an airfoil characterized as a deviation from straight as a either a fraction of the chord length or percent of a chord length (e.g., 0.01 c or 1%)

CFD = computational fluid dynamics

c, Chord = chord, distance from leading edge to trailing edge of an airfoil or wing

$Drag_{form}$ = form drag, which herein is the drag due to pressure on the surface

$Drag_{total}$ = total drag as equal to sum of form and shear drag

L/D = lift-drag ratio, the primary measure of airframe efficiency; ***L/D*** is calculated as the CFD lift coefficient divided by the drag coefficient.

lift pressures = pressures that generate aerodynamic lift such as lower pressures on upper surfaces and higher pressures on lower surfaces.

NACA0006 = an airfoil shape defined by NACA standards with a t/c of 0.06

P = pressure (N/m^2)

PIC = particle image velocimetry

S, dS = surface area (m^2) and differential surface area

Source = Source with a capital "S" refers to a source of thrust.

STL = stereolithography, file generated by computer aided design software

U, ***u*** = velocity.

SUSAN = SUbsonic Single Aft eNgine

t/c = thickness to chord ratio, thickness is a maximum vertical dimension

VTOL = vertical takeoff and landing

F20EI3xxx = Airfoil catalog code for Figures 5-12. F_dd_NN_n1_Deg_n2_***L/D***_n3, where: F is February of 2023, dd is the day, NN is the leading edge or ellipse specification, n1 is camber in percent, n2 is α_A in degrees, n3 is the ***L/D***. Minor variations in code can be interpreted from the Figure caption.

α_A = angle from horizontal (°), subscript A identifies an airfoil pitch angle with nose up as positive

α_P = angle from horizontal (°), subscript P identifies angle of a point on a line or surface

Introduction

THIN-plate cambered wings are of particular interest in solar aircraft since solar panels may be modified to function as ultralight thin cambered wings. Bifacial plate compatibility can increase the productivity to values not attainable on earth's surface, [1, 2] and lower lift coefficient constraints that are problematic with contemporary aircraft are compatible with high surface areas for solar panels. In high altitude platform (HAPS) applications, wing loadings of less than 4 kg/m^2 often translate to steady-flight lift coefficients less than 0.2, which opens the door to thin cambered wings not suitable for many contemporary aircraft.

Figure 1 illustrates a thin cambered panel configured as a thin-plate cambered wing section. The configuration is like a cloth across the frame of a hang glider, only there is a higher payback for better engineering to achieve and maintain higher ***L/D***.

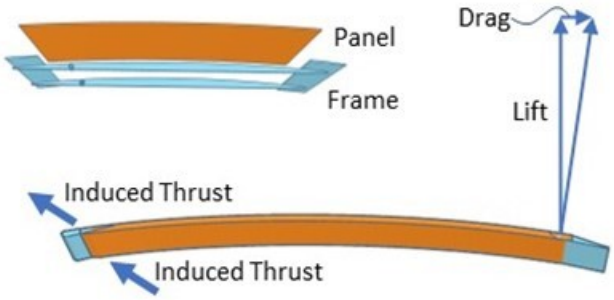

Fig 1. Illustration of panel as thin-plate cambered airfoil

Factors that favor the use of thin-cambered bifacial solar panels on aircraft relative to surface installations include:

- About 20% more radiation at higher altitudes than on Earth's surface.
- An additional 30% to 90% productivity from bifacial panels (versus ~23% max on surface). [2, 3]
- Displacing the costs and weights of batteries or fuel on aircraft versus displacing grid electricity costs on Earth's surface.
- Extended hours of sunlight as possible when flying with Earth's rotation.
- A lack of blockage from clouds, snow, and vegetation which can add on average another 30% to the solar productivity versus Earth's surface.
- Quick-connect mechanisms can eliminate much of the installation costs since aerodynamic lift supports the weight and orientation after takeoff.
- Aircraft applications avoid greenfield or brownfield construction costs as well as maintenance related to dust, vegetation, and snow.

Preliminary estimates identify the best applications as having payback periods of less than a year for the net costs of these solar capabilities over a base case aircraft design. The payback periods will continue to decrease with improving

photovoltaic cells. An improved understanding of thin cambered airfoils is needed to best enable these applications.

A goal of this paper is to summarize an improved understanding as a list of heuristics that can be continuously improved. Heuristics advance fundamental equations, that can be difficult to relate to designs, into practical concepts that the human mind is better able to coalesce into new designs and innovations.

The chemical engineering heuristics as compiled by Walas in chemical engineering are the result of thousands of man-hours of experience. That approach is not possible here. Alternatively, computational fluid dynamics (CFD) is used to establish trends in performance which are converted to heuristics.

Background

The introduction and development of CFD has expedited pre-prototyping airfoil, wing, and aircraft optimization. Wind tunnel testing has repeatedly validated CFD as an accurate pre-prototyping tool, including techniques such as particle image velocimetry (PIV) [4], which defined and identified pressure and vortex instabilities that can progress forward on the lower surface of a wing. This has led to the extensive study and definition of instabilities and flow behaviors on wings [5]. These pressure distributions are impacted more from the Reynold's number and flow rate than the turbulence experienced on the wing [6]. 2D CFD airfoil simulations at steady-level conditions is less demanding than the more-complex dynamics 3D studies of wings, with airfoil simulation routinely accepted as fundamentally accurate. [7-10]

This current work emphasizes interpretation of 2D airfoil pressure profiles rather than velocity profiles. Pressure differences are both the cause and effect of both turbulence and velocity streamlines; they also directly determine lift and ***L/D***. This paper uses pressure profiles to provide an improved understanding of air foil technology with an emphasis on thin-plate cambered airfoils.

Using computational fluid dynamics, cambered airfoil designs have advanced. Osei has developed a cambered airfoil with the potential of reaching an ***L/D*** up to 135, with theoretical ***L/D*** maximum listed around 155 with further optimization [11]. Lee et. al.[12] focused on velocity profiles; those velocity profiles provide similar information and results as pressure profiles.

A thin-plate cambered airfoil has about 90% of the chord at a constant thickness as characterized by a thickness-to-chord ratio ("t/c"). Specification of a thin-plate cambered airfoil includes specifying t/c, camber, and the detailed shape of leading and trailing edges. The shapes of leading and trailing edges encompass several additional design degrees of freedom.

There is significant potential for the use of learning algorithms to adjust and optimize the shape of airfoils using CFD.[13] Through the development and testing of airfoils with morphing trailing edges, Wu is able to identify how minor differences in otherwise similar shapes has a noticeable impact on ***L/D*** in both physical and computational experiments, reaching theoretical ***L/D***s of 80 by minor adjustments to the trailing edge. [14] In an ideal design process, heuristics quickly identify base case designs and learning algorithms refine the design with details enabling ***L/D*** > 60.

Achieving high ***L/D*** in a wing's airfoil cross sections is a necessary, but not sufficient, condition to achieve high ***L/D***. Air flow across side edges causes 3D wings to have lower ***L/D*** than the ideal-case 2D airfoils which do not account for side-edge losses.

In low ***AR*** wings, losses of lift pressures around side edges tend to dominate overall ***L/D*** performance. Distributed propulsion has the ability to mitigate these losses. This paper provides preliminary 2D airfoil performance data on use of distributed propulsion to achieve high ***L/D*** in low ***AR*** airframes.

One expression of NASA's SUSAN concept [7, 8] uses an engine placed aft a tubular fuselage to power sixteen electrofans distributed on the lower surface of the wingspan of an otherwise contemporary fuselage-wing aircraft architecture—a 50% reduction in emissions per passenger mile is identified as a realistic goal for SUSAN. [7] Hybrid wing-body designs identify using the combination of distributed propulsion along the trailing edge of the fuselage in combination with wingtip engines to attain a 70% fuel burn reduction. [15] These increases in efficiency suggest that distributed propulsion can be used to achieve high ***L/D*** in low ***AR*** airframes.

Reviews of distributed propulsion [16] identify the most common use of distributed propulsion as spread along midboard wing sections and on trailing edges of lift-producing surfaces. The review by Gohardani dates distributed propulsion to 1924 including 20 different milestones, [17] In a 2022 review of future aircraft concepts, McDonald et al identified contemporary tube-wing, delta/flying wing, helicopter, quadcopter, Bee/Bird, and other multicopter configurations. [18] Instant concepts using long-chord edges on low ***AR*** designs were not considered and have not been documented in literature outside a few recent patent applications. [19] A similar review by Finger did not include novel approaches suitable for instant designs targeting high ***L/D*** low ***AR*** aircraft. [20]

None of the prior art identify designs using thin-plate cambered airfoils. Establishing good heuristics on use of thin-plate cambered airfoils prior to considering uses with distributed propulsion could expedite progress on the design of high ***L/D*** low ***AR*** airframes.

Borer (2017) identifies "the benefits of distributed propulsion have been hypothesized and demonstrated, they

have largely not yet been reduced to a series of cogent design rules and heuristics that are typically necessary to begin the aircraft design process". [21, 22] Borer initiates work in related heuristics, but those heuristics are based on different analyses and are not as fundamental as those summarized at the end of this paper.

Russo et. al. studied the impact of a Source in front of a contemporary airfoil. Heuristics were not used in identifying that base case design. Impact of the Source on lift and drag were evaluated, but the impacts were not evaluated on a level to advance heuristics that could be more-broadly applied. Also, gain-loss analyses, (i.e., gains from reduced drag versus losses from reduced thrust), were not performed.

Methods

CFD calculations were performed using SimFlow's Airfoil simulation feature. The airfoil model data files used for SimFlow were either data files of coordinates or STL files that can be generated from a variety of software packages.

Pitch angles for an airfoil (α_A) are the angle from horizontal (nose-up as positive) of the airfoil's chord, where the chord is a straight line connecting the leading and trailing edges. In 2D simulations, the pitch angle of a point (α_P) on a curved line is the angle of the line tangent to the curve at the point of interest.

Air angle of attack (AoA) is the angle at which air's free stream velocity vector approaches the surface. Pressures near a surface can change air's velocity vector (i.e., bend the air's flow), and so, the AoA can change as it approaches a surface.

A camber line is the line vertically halfway between the upper and lower surface from leading to trailing edge. The upper surface, lower surface, and camber line are considered to have the same camber for airfoils of this paper, and the term "thin-plate cambered airfoil" and "thin cambered airfoil are used synonymously. Camber and thickness of an airfoil are typically specified as a fraction or percent of the chord length and may be abbreviated. A camber of 0.03 is also referred to as a 3% camber.

All images of pressure profiles use the symmetric color scale of Fig. 2 with pressure in Pascals.

Results

Fundamental Driving Forces for Lift

The CFD pressure profiles for a symmetric contemporary airfoil (modified NACA0006) are provided by Fig. 2.

These profiles provide good insight into the aerodynamic phenomena that generate lift forces; the term "lift forces" cumulatively refers to higher pressures on lower surfaces and lower pressures on upper surfaces; both create upward vertical force on an airfoil.

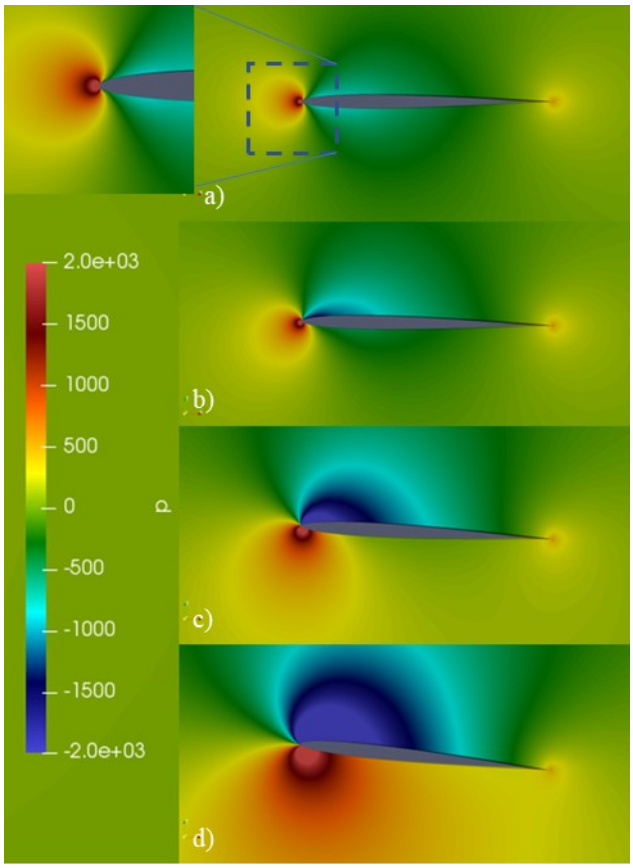

Fig 2. Pressure (Pa) profiles of a modified NACA0006 airfoil at pitch angles relative to free stream velocity. of a) 0°, b) 1°, c) 3°, and d) 6°. Air velocity is 90 m/s and respective *L/D* of 0, 15, 37, and 50.

At 0° α_A, (Fig. 2a) the freestream velocity impacts the leading edge to create a high-pressure "bubble" (red) immediately in front of the leading edge with a horizontally symmetric pressure profile for a horizontally symmetric NACA0006 airfoil. Proceeding to the trailing edge from the pressure bubble, the following occurs:

a) The pressure bubble in combination with the shape of the leading edge create a lower-pressure region (blue) due to velocity vectors diverging from the surface.

b) The lower-pressure bubble bends velocities back toward the surface to create progressively increasing pressures (blue to green to yellow).

c) After the trailing edge, velocity trajectories of air converge to create a higher-pressure turbulent region behind the trailing edge.

As $\boldsymbol{\alpha_A}$ is increases (Fig. 2b-d) the magnitude of the leading-edge lower-pressure bubble increases over the upper surface. Lower pressures on the upper surface pull in air from afore and below the leading edge; this shifts the location of the leading-edge pressure bubble to surfaces progressively lower on the airfoil's lower surface.

On the upper surface at approximately 0.1c from the leading edge, the lowest pressures form at $-1° < \boldsymbol{\alpha_P} < 1°$. Applying the definition that lift is a vertical force and drag is a horizontal force, Equation 1 identifies how $\boldsymbol{\alpha_P}$ is the primary factor that determines ***L/D***. The concentration of lift forces between $-1° < \boldsymbol{\alpha_P} < 1°$ locations is a critical geometric feature to achieve localized ***L/D*** > 60.

$$Lift = \Delta P\, \Delta S\, Cos(\alpha_P); \quad Drag_{form} = \Delta P\, \Delta S\, Sin(\alpha_P); \quad L/D = \frac{1}{Tan(\alpha_P)} = \frac{57}{\alpha_P^{\circ}}\ at\ low\ \alpha_P \qquad (1)$$

where ΔP is local pressure minus free stream pressure, ΔS is change in surface area, form drag is total drag less shear drag, and Lift and Drag are for the surface defined by ΔS.

At $\boldsymbol{\alpha_P} < 0°$ drag is negative ("induced thrust"). Induced thrust counteracts other drag sources in ***L/D***. A small decrease in the "D" denominator term can lead to significant increases in ***L/D***. Induced thrust commonly occurs on aircraft wings and is vital toward achieving ***L/D*** > 40.

The Fig. 2 transformation of the NACA0006 airfoil as pitch ($\boldsymbol{\alpha_A}$) increases from 1° to 6° includes: a) increasing lift pressures with respective increasing lift coefficients, b) a concentrating of lift pressures at $-1° < \boldsymbol{\alpha_P} < 1°$, c) transferring of the pressure bubble from a position of creating purely drag force to a position with substantial lift force, and d) forming of induced thrust at the foremost part of the low-pressure bubble. This transformation creates an ***L/D*** and stability profile for traditional airfoils beyond what would be expected based on inspection of the airfoils. Antiquated theories (i.e., Bernoulli or momentum theories of lift) do not even address ***L/D***.

Figure 3 illustrates a 0.01 t/c thin flat plate airfoil (i.e., most of airfoil is at a constant thickness of 0.01 c). The airfoil has a rounded leading edge and an asymmetric trailing section where the lower surface is at the same $\boldsymbol{\alpha_P}$ as the mid-chord area, placing all the taper on the upper surface. The asymmetric taper creates a lower pressure on the upper surface that transforms pressure profiles to desirable lift pressures throughout the airfoil. This transformation illustrates how a source of low pressure that draws air at the speed of sound can: a) overcome subsonic free stream velocities, b) transfer the leading-edge pressure bubble to a lower, preferable position and c) create higher pressures on lower surfaces. This transformation is not predicted by antiquated theories of lift.

Figure 3 illustrates how strong lift forces can be generated by a flat plate airfoil; As all the surfaces are at the same $\boldsymbol{\alpha_P}$, Equation 1 can be applied to the flat-plate airfoil in its entirety. At $\boldsymbol{\alpha_A} = 6°$ the 9.5 ***L/D*** for the flat plate

airfoil is a rather poor value.

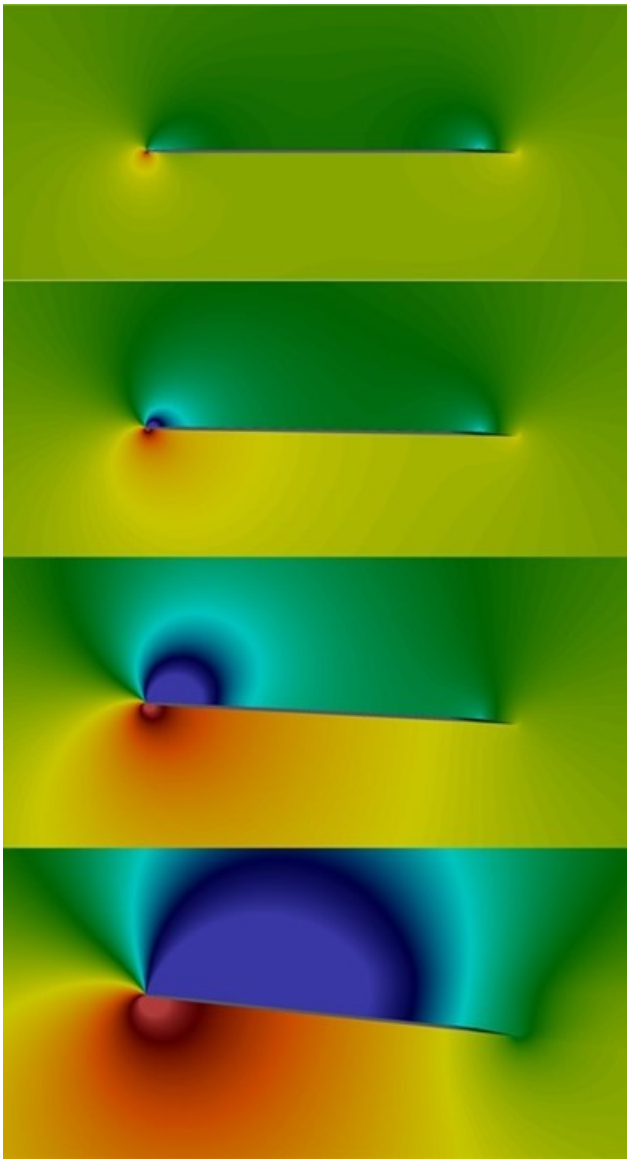

Fig. 3 Pressure (Pa) profiles of a 0.01 t/c flat plate airfoil with rounded leading edge and upper taper at trailing edge. Airfoil pitch angles are a) 0°, b) 1°, c) 3°, and d) 6°'; air velocity is 90 m/s for c = 1 m; and respective *L/D* are 16.8, 24.5, 17, and 9.1.

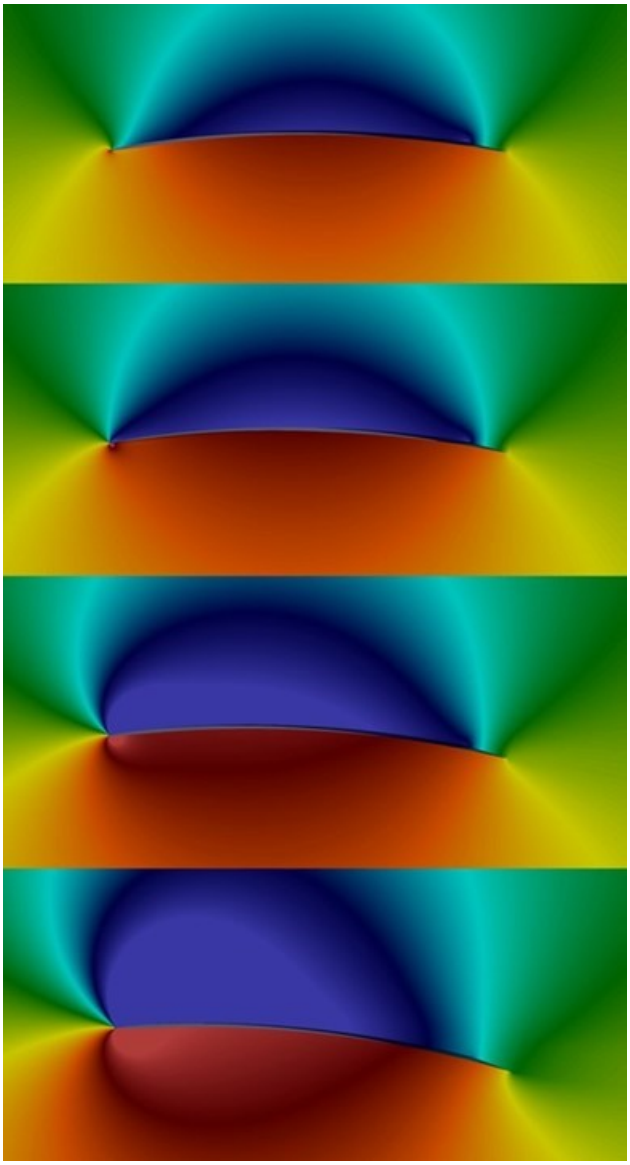

Fig 4. Pressure (Pa) profiles of a 0.01 t/c 3% cambered airfoil at 90 m/s at α_A of 0°, 1°, 3°, and 6°.

Figure 4 illustrates pressure profiles for a thin-plate cambered airfoil. Thin-plate cambered airfoils have a substantially constant thickness versus airfoils like the NACA0006 airfoil ("contemporary airfoils") that have definitive maximum in thickness at 0.12 c.

The following trends are observed for thin-plate cambered airfoils versus contemporary airfoils:

a) lift pressures are more-evenly distributed,

b) higher pressures on lower surfaces contribute more to the total lift,

c) for low range cambers (sub 6-10%), the magnitudes of lift and lift coefficients increase with camber,

d) induced thrust magnitudes can be substantial which critically compensate for lift pressures and associated form drag at $\alpha_P > 2°$, and

e) the continuous camber on upper and lower surfaces of a thin-plate cambered airfoil continue to bend air as it progresses toward the trailing edge resulting in extended lift pressure surfaces.

Screening Studies

Screening studies on thin-plate cambered airfoils (0.001 t/c) evaluated α_P of 0°, 1°, 2°, and 3°; and cambers of 1%, 2%, 3%, 4%, 6% and 10% of the following geometries:

- increased leading camber (Fig. 5)
- increased trailing camber (Fig. 6)
- symmetric increased edge cambers (Fig. 7)
- constant arc camber (Fig. 8)

All airfoils with an increased camber only on the leading edge exhibited a reverse-lift pressure profile at the leading edge, characterized by a low-pressure region below the leading edge and high-pressure region above the leading edge.

Several of the airfoils of Figs. 6-8 were able to achieve higher pressures throughout the lower surface and lower pressures throughout the upper surface. The constant arc airfoils of Fig. 8 achieved greater magnitude ΔP in the midsection; and consequently, the constant arc airfoils exhibited relatively low induced thrust with correspondingly lower ***L/D***.

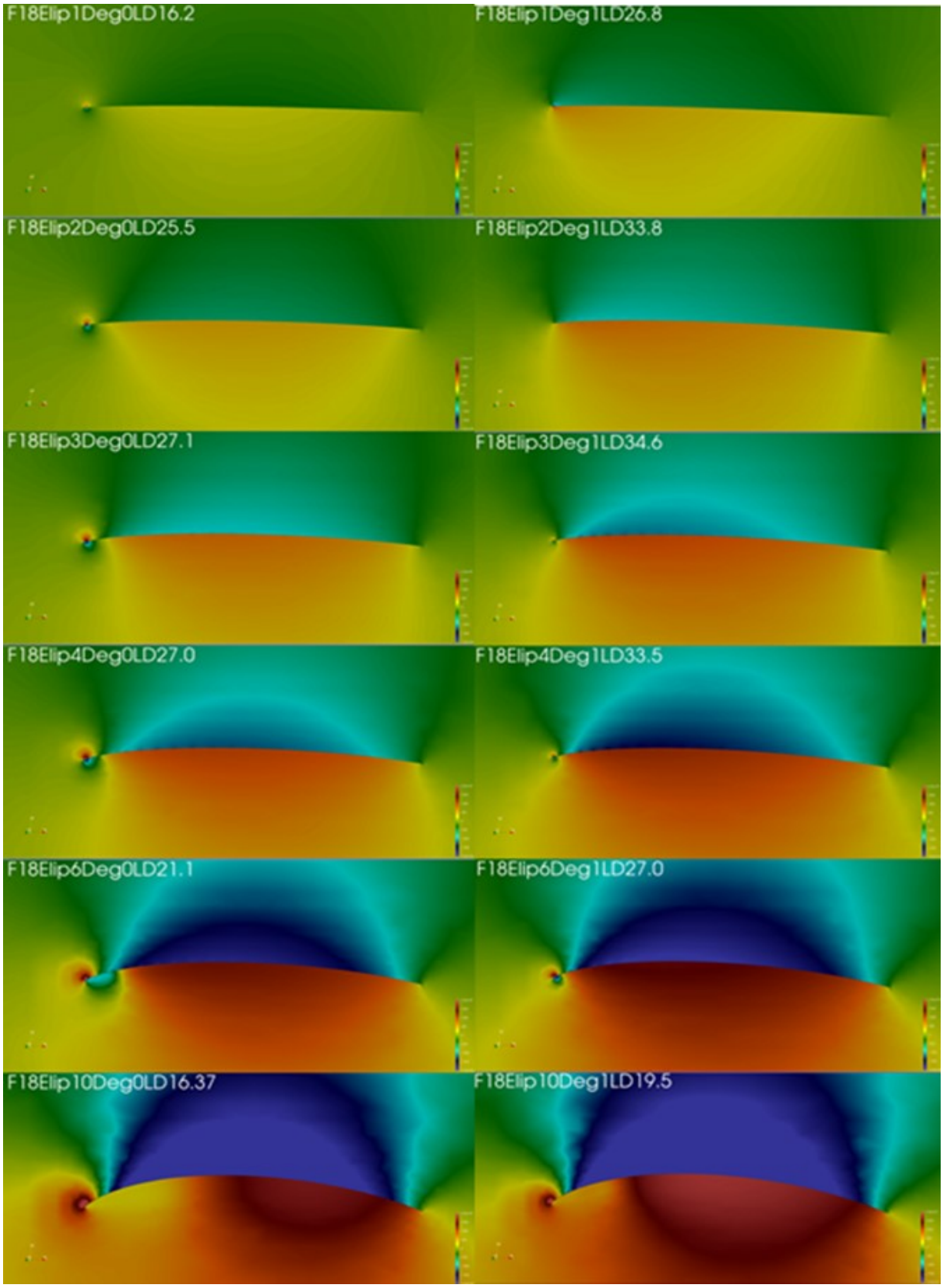

Fig. 5 Pressure profiles of thin airfoils with increased leading-edge camber.

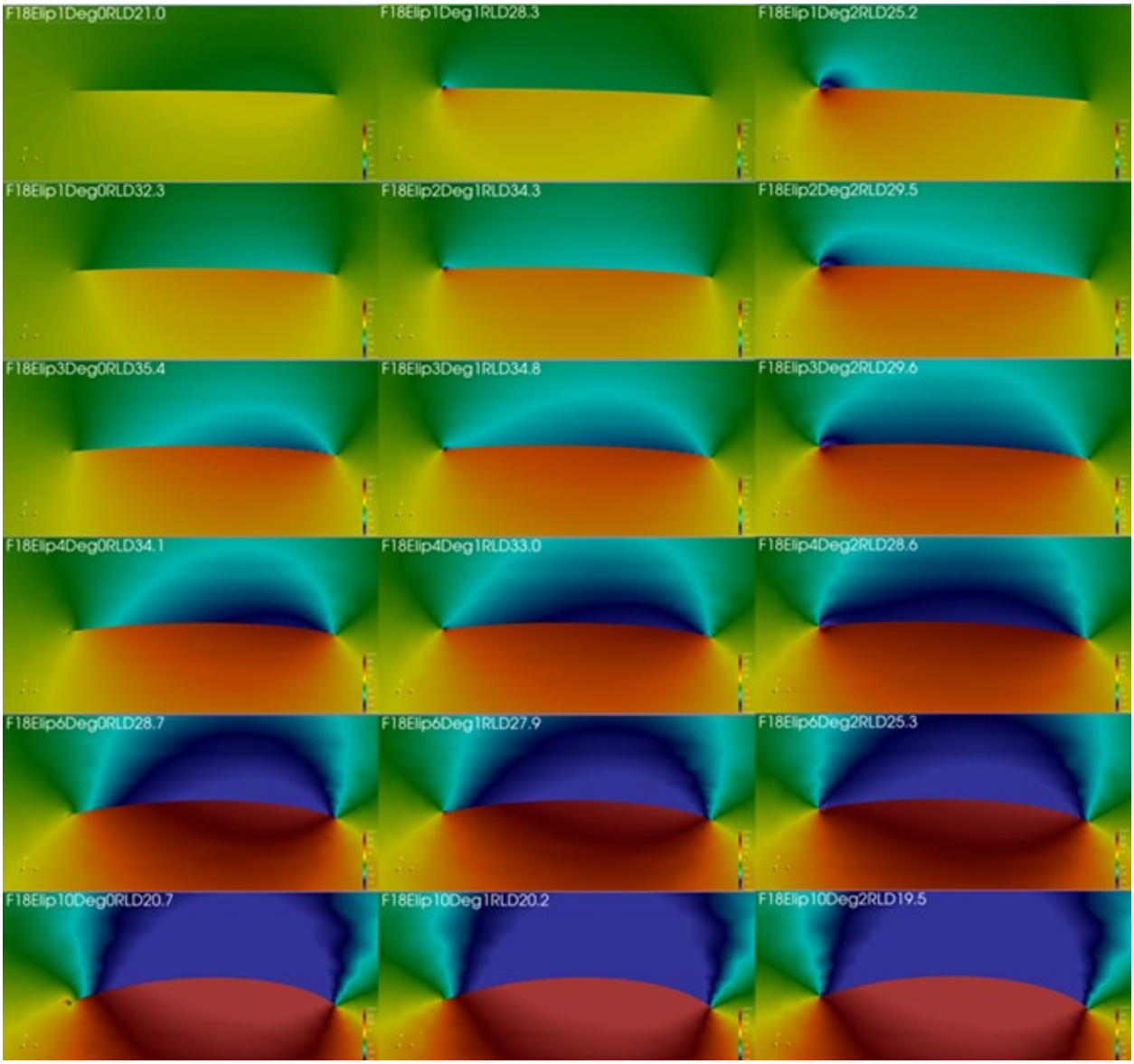

Fig 6. Pressure profiles of thin airfoils with increased trailing-edge camber.

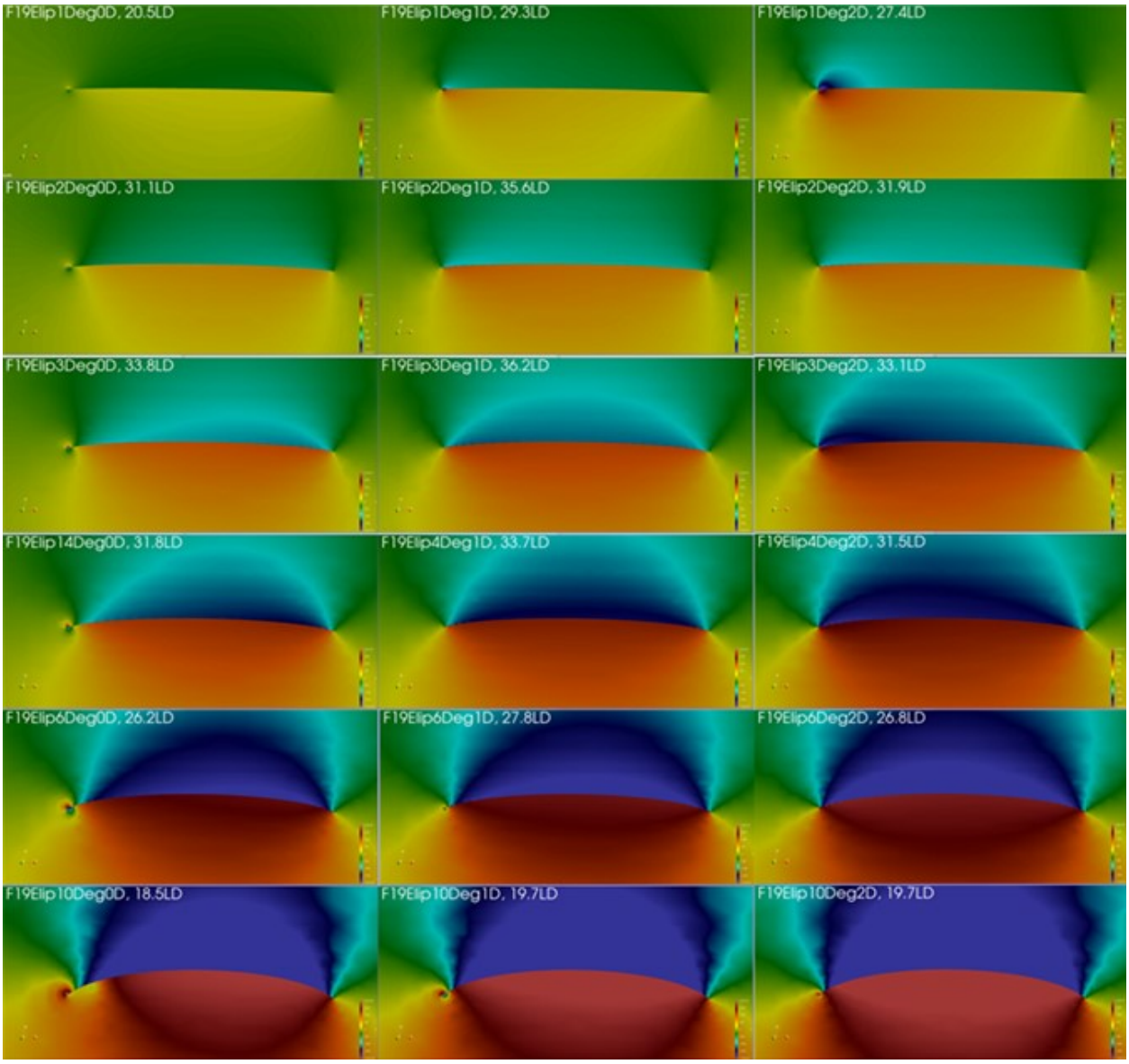

Fig. 7 Pressure profiles of thin airfoils with symmetrically increased camber on edges.

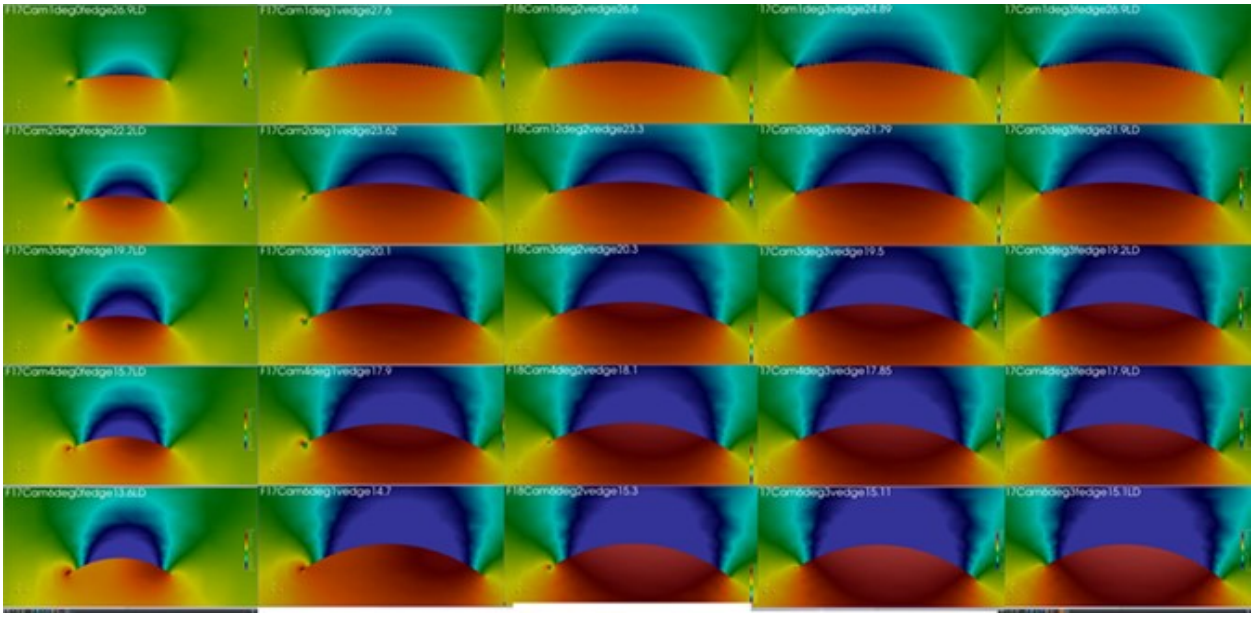

Fig. 8 Pressure profiles of thin airfoils with constant arc camber.

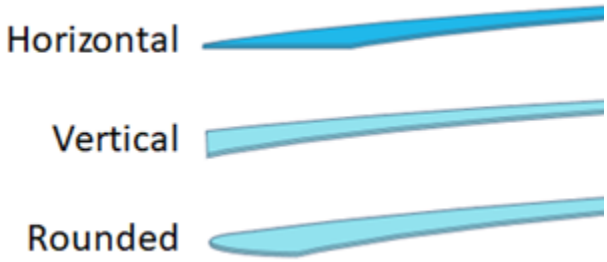

Fig. 9 Leading edge shapes

The airfoils with an increased camber only on the trailing edge exhibited a greater tendency to have higher pressures on the lower surface of the trailing edge versus the leading-edge lower surface. This created a bias against fully developing induced thrust from the leading edge and corresponds with lower ***L/D***. Further studies were performed on the symmetric camber; no basis was provided that symmetric camber would be preferred to asymmetric increased edge camber airfoils.

The constant arc camber airfoils of Fig. 8 were also evaluated with different transitions from upper to lower surfaces at the trailing and leading edges. Figure 9 illustrates leading edge transitions; trailing edges were evaluated at vertical and horizontal transitions. Changing the trailing edge had minimal impact with < 0.1 ***ΔL/D***.

Versus leading-edge studies, a lower emphasis was placed on parametric studies to evaluate how the taper of the trailing edge impacted ***L/D***, with a default geometry of an upper surface taper to a point (in 2D airfoil space). At

airfoils having <0.001 t/c, the impact of shape of the leading edge tends to be negligible.

Impact of Leading-Edge Shape and Thickness

The performance of horizontal straight (Fig. 10), vertical straight (Fig. 11), and rounded (Fig. 12) leading edges were compared at 1% to 4% t/c and 0° and 2° α_A. At t/c > 0.01, the shape of the leading-edge impacts ***L/D***. The 1% t/c airfoils had leading-edge reverse lift at 0° with higher pressures on upper surfaces and lower pressures on lower surfaces, and all performances at 2° exhibited desirable lift at the leading edge. The best ***L/D*** were at about 0.5° α_A.

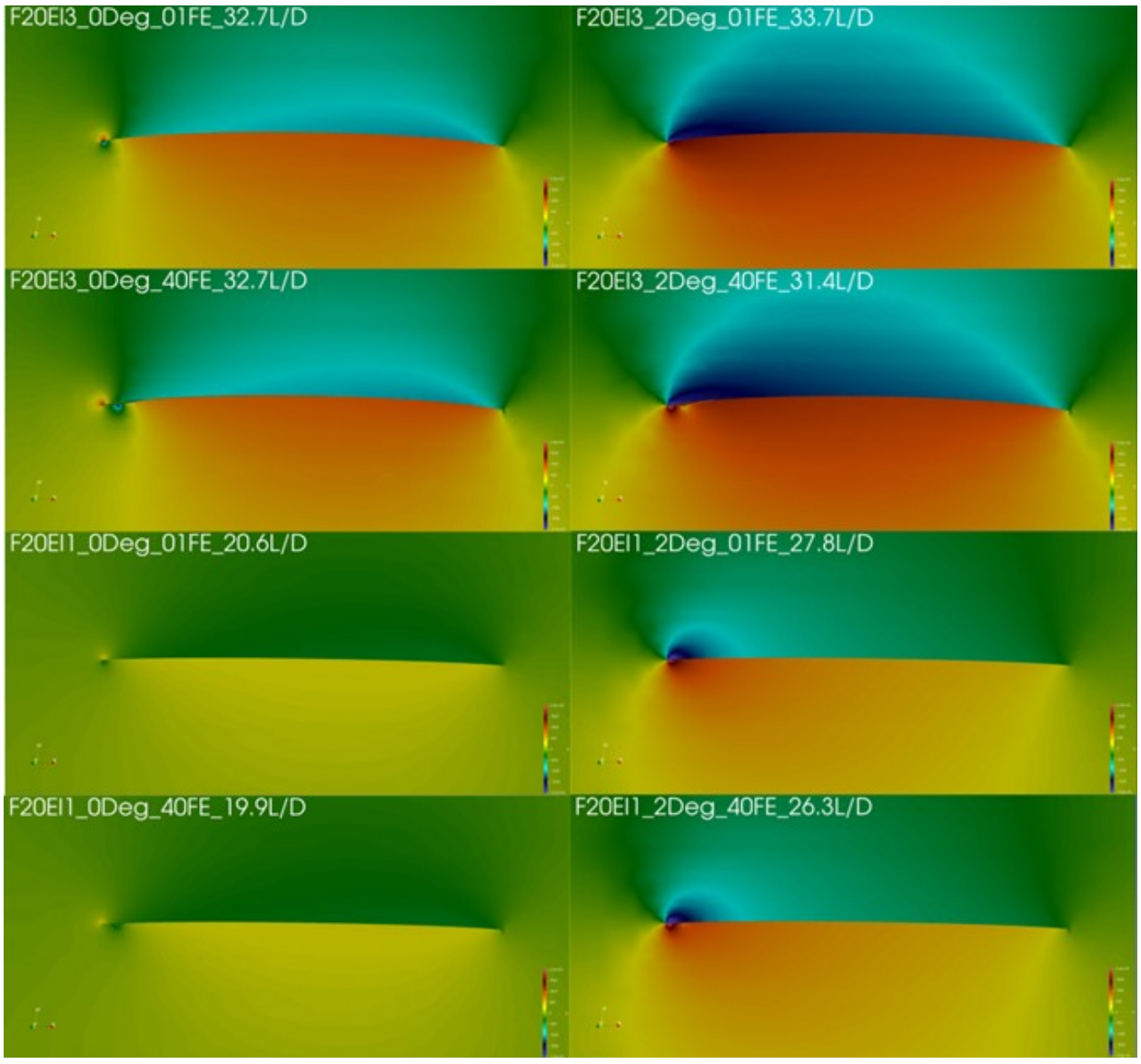

Fig.10 Pressure profiles for horizontally flat leading edge transition from upper to lower surfaces at horizontal distances of 1% and 4% t/c at 0° and 2° α.

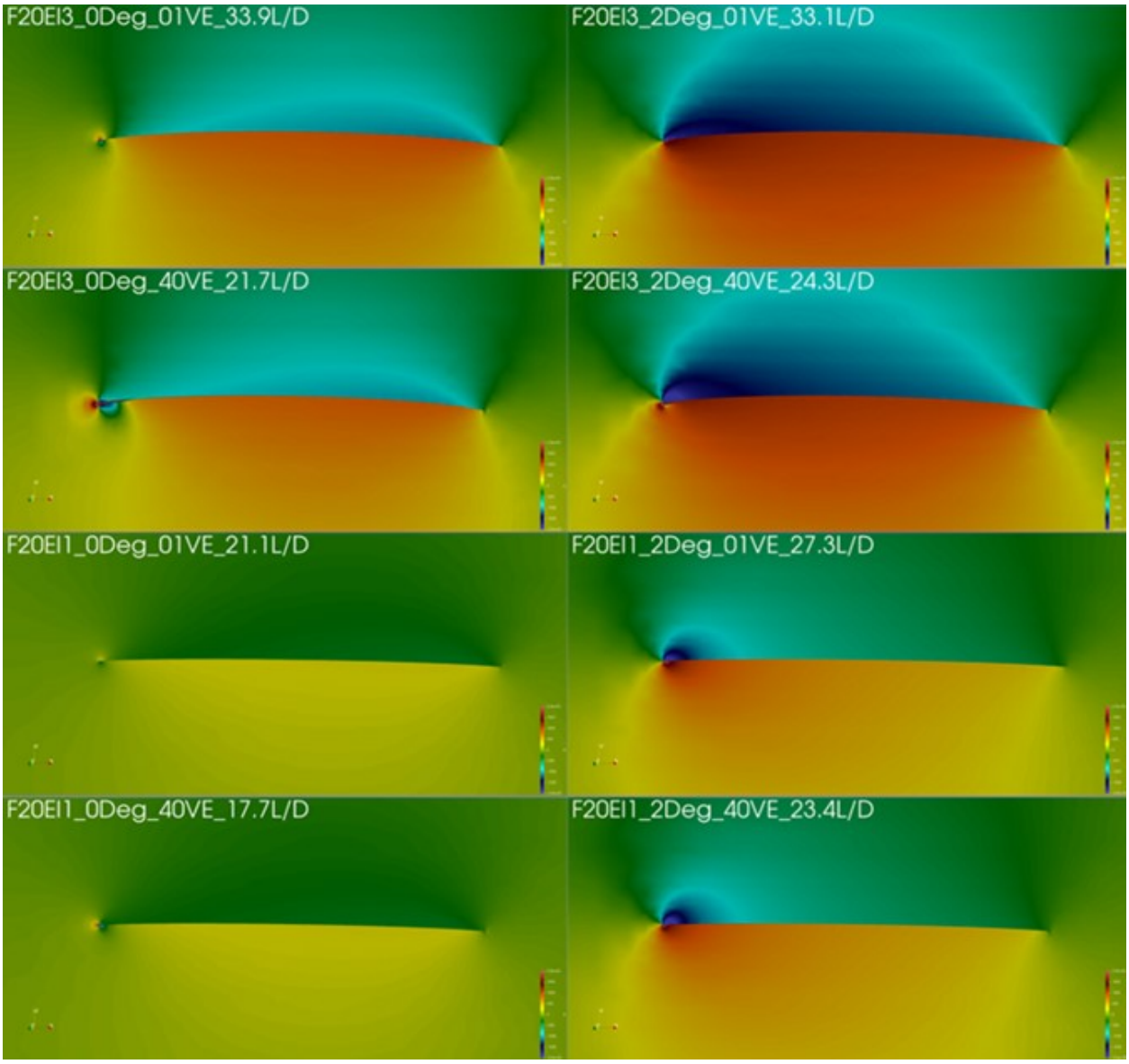

Fig. 11 Pressure profiles for vertically flat leading-edge transition of Fig. 9 airfoils

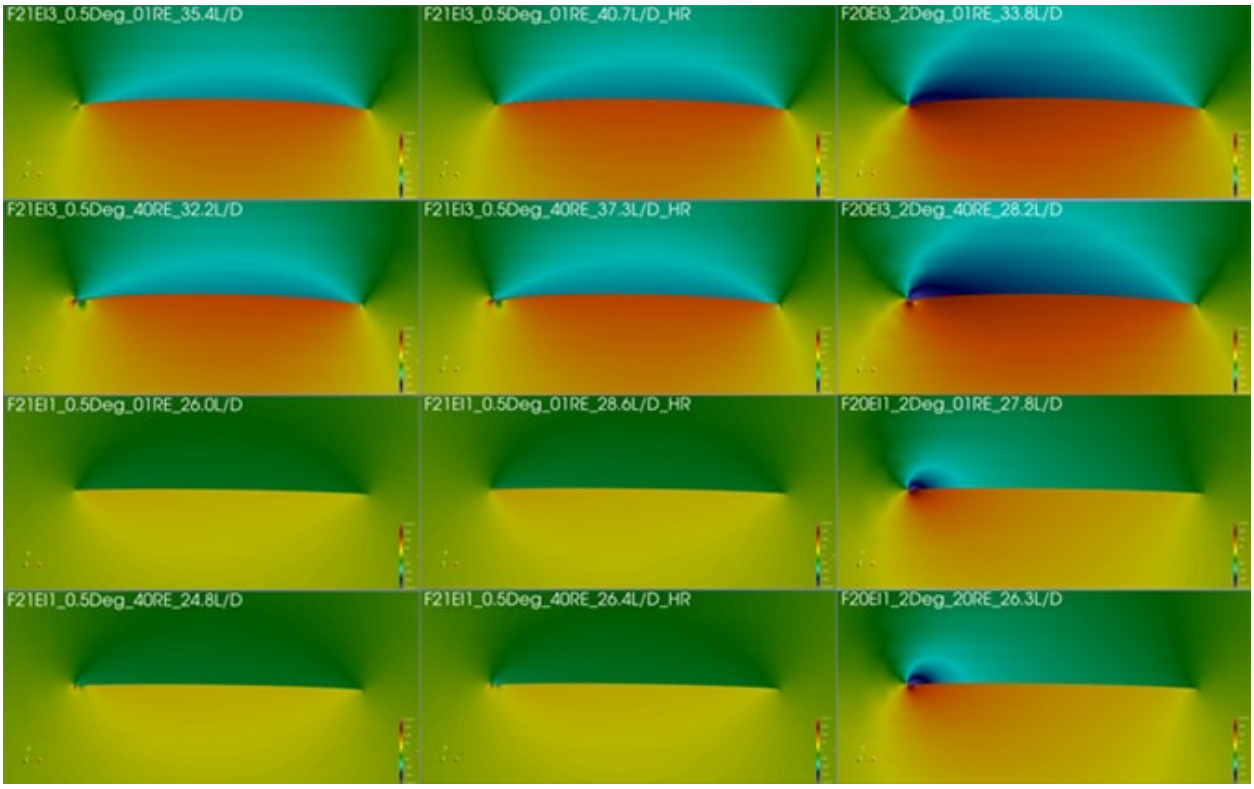

Fig. 12 Pressure profiles for rounded leading-edge transition of Fig. 9 airfoils. CFD studies at 0° α failed to converge, and so, 0.5° was used.

The vertical leading edge was systematically worse than horizontal or rounded leads. The leading-edge shape has fundamental influence on both creation of velocity vectors diverging from the surface above the leading edge and successful expansion of the pressure bubble. Induced thrust is created by the pressure bubble as it expands into the forward most part of the lower surface. The vertical leading edge has no inherent mechanism to promote or direct airflow for inducing thrust, thus leading to the worst performance.

Rounded leading edges performed slightly better than the horizontal, but performances differences were within the accuracy of the simulations.

A near optimal leading-edge configuration has a NACA00XX series rounded leading edge as provided by Equation 2. [23]

$$y_t = 5t\left[0.2969\sqrt{x} - 1.260x\ - 0.3516x^2\ +\ 0.2843x^3 -\ 0.1015\,x^4\right] \tag{2}$$

where:

x is the position along the chord from 0 to 0.12 c,

y_t is the half thickness at a given value of x (centerline to surface),

t is the maximum thickness as a fraction of the chord (so for a 0.01 c thin-plate airfoil, t is 0.01).

The trailing edge configuration is as provide by Equation 3

$$y_t = 1.0 - 5t\left[0.2969\sqrt{z} - 1.260z - 0.3516z^2 + 0.2843z^3 - 0.1015\,z^4\right]$$

for $$x = \frac{0.10}{0.88}\,z + \frac{0.78}{0.88} \qquad (3)$$

where z is a substituted variable going from 0.12 to 1.0 in defining x from 0.90 c to 1.0 c.

From 0.12 c to 0.90 c, $y_t = t$. These equations provide a thin-plate airfoil of unit length; the size is scalable. The results summarize by Figure 4 are with this near-optimal leading-edge shape.

Figure 13 summarizes the impact of thickness, t/c, on the magnitude of the pressure bubble where higher pressures in front of the leading edge decrease ***L/D***. Optimal rounded leading edges tend to have peak ***L/D*** values at 1% to 2% t/c. Airfoils of similar camber and $\boldsymbol{\alpha_A}$ had similar ***L/D*** at 0.1% t/c (i.e., leading and trailing edges had minimal impact).

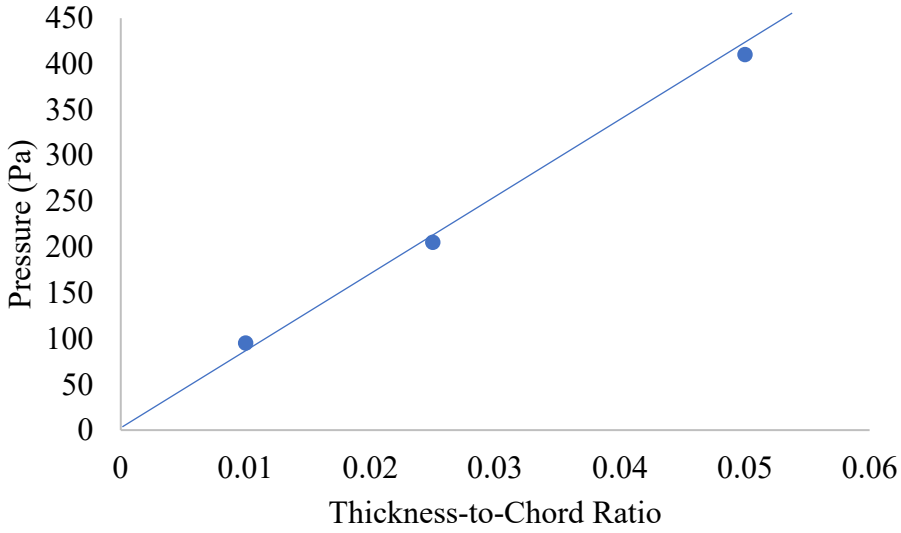

Fig. 13 CFD calculated pressures at a distance 0.2 chords in front of the leading edge of 0.02 c thin plate camber at 90 m/s and one atm ambient pressure.

Preliminary Data Source-Augmented *L/D* – A key observation starting with Fig. 2 is the manner in which a source of low pressure at a trailing section can propagate and change pressure profiles throughout an airfoil. The intake and discharge of propulsors are sources of lower and higher pressures, respectively. Hence, a thrust source, hereafter "Source", can be used to impact pressure profiles and respective lift and drag forces. Figure 14 summarizes pressure profiles for a Source at different power settings on the trailing edge of the upper surface of an airfoil of 0.01 camber at $\alpha_A = -1°$ (i.e., pitch).

When the Source is off, free stream velocities generate a pressure bubble on the upper surface of the leading edge. The slight camber at the leading edge blocks free stream velocity vectors from directly impacting the lower surface; as a result, air's velocity diverges from the lower surface to create lower pressures on the lower surface near the leading edge.

The upper-surface taper near the trailing edge generates a lower pressure that expands to generate lift, but that lift is minimal compared to the negative lift pressures on most of the airfoil surface.

The ***L/D*** constantly increases with increasing trailing-edge Source power, with ***L/D*** increasing from -1.49 to 49.5 as the power setting is increased from 0 to 80 m^4/s^2. The following patterns can be observed with increasing Source power: a) the low-pressure region fore the Source increases in magnitude and expanse; b) the leading-edge pressure bubble transitions to the lower surface where the higher pressures generate lift and minimal drag; and c) the higher pressure region on the lower surface expands from leading to trailing edge.

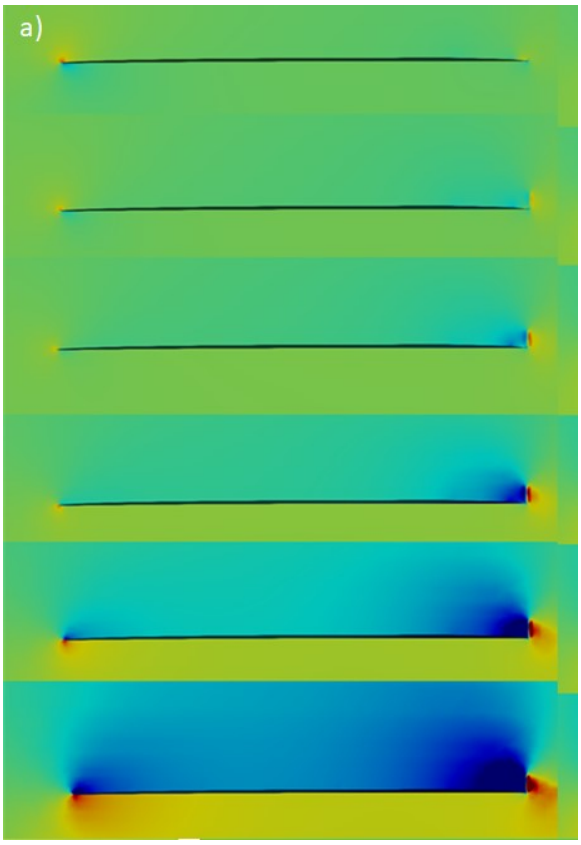

Fig. 14. Pressure profiles for an airfoil of 0.01 c camber and αA = -1° and trailing-edge upper-surface Source.‡

‡ From top to bottom, the Source power settings are 0, 5, 10, 20, 40, and 80. ***L/D*** values are: a) -1.49, 5.36, 11.0, 20.0, 33.3, and 49.4

The trailing-edge upper-surface Source is very effect

tive for increasing ***L/D*** of the airfoil of the Fig. 13 pressure profiles. The primary factors causing this high efficacy are the vector forces identified by Equation 1. The Heuristics resulting from these observations are able to qualitatively predict that behavior impact of the Source on airfoil ***L/D***. However, the use of Sources to increase ***L/D*** has complexities and implications beyond the heuristics designed to assist in effective use of Sources to realize high ***L/D*** low ***AR*** airframes. Those additional topics are beyond the scope of this paper.

Discussion

Overarching Trends

Table 1 compares the ***L/D*** for the flat plate airfoil of Fig. 3 and the cambered airfoil of Fig. 4. It illustrates how the Equation 1 "geometric mandate" ultimately hinders the performance of a flat plate airfoil at increasing α_A.

Table 1 Comparison of flat plate, ideal Equation 1 flat plate, and and 0.03 camber 0.01 t/c airfoil with increasing camber at leading and trailing edges and an Equation 3 leading edge shape.

Pitch Angle (°)	Flat Plate C_L	Flat Plate ***L/D***	0.03 Camber C_L	0.03 Camber ***L/D***	$\alpha°_A$ / 57.3
0	0.047	16.8	0.652	67.5	0
1	0.15	24.5	0.752	66	57.3
3	0.36	17	0.919	41	19.1
6	0.73	9.1	1.09	18.7	9.55

Thin flat plate airfoils are substantially absent surfaces conducive to induce thrust. A trailing-section asymmetric creates lift at $\alpha_A = 0°$, but the lift coefficient is very low at 0.047. As $\alpha_A = 0°$ increases, the ***L/D*** of a flat plate airfoil approaches a simple relation of ***L/D*** = $\alpha°_A$ / 57.3.

The induced thrust created by leading edge lower pressures is a critical feature enabling contemporary airfoils to achieve high ***L/D***. Similar to contemporary airfoils, well-designed cambered airfoils are able to capitalize on induced thrust to increase ***L/D***. Lift coefficients increase with increasing camber and $\alpha°_A$ for higher ***L/D*** thin-plate cambered airfoils.

Continuously curving surfaces, like a cambered surface, prevent the formation of straight-parallel flow and improves ***L/D***. Also, as the camber of a thin plate airfoil approaches 0 (i.e., a 0.01 c), the upper limit of performance will be limited by the Equation 1 geometric mandate.

Many of the pressure profiles of this paper show decreasing lift pressure magnitudes lower surfaces near the

trailing edge. Air has a driving force to expand from higher to lower pressures; the pressure gradient for this driving force on trailing edges of airfoils will be higher than through the rest of the airfoil unless pressure is generated near the trailing edge. Higher $\boldsymbol{\alpha_P}$ at trailing edges will generate higher pressures faster to compensate for the tendency to expand, but this is at the cost of higher trailing section form drag. Other origins of pressure generation include collision of upper surface with lower surface velocities which converts dynamic pressure into static pressure; this tends to occur with upper-surface trailing-edge Sources and greater tapers in thickness at trailing edges.

Unlike side-edge phenomena, which will not manifest in 2D CFD simulations, 2D CFD simulations account for trailing edge effects.

Trends in Performance

Four types of camber were evaluated over a series of angles and cambers in thin-plate airfoils. The following were the findings:

1. From greatest to least maximum ***L/D***, the order was cambered airfoils having: a) increased camber at front and back, b) increased camber at back only, c) increased camber at front only, and d) even camber throughout the arc.
2. An even distribution of pressure on both upper and lower surfaces was able to be achieved at maximum cambers of 2% to 4% and 1° α_p with increased camber on both front and back.

Four leading edge thicknesses (0.001, 0.01, 0.02, and 0.04) and three leading edge shapes were evaluated (flat horizontal, [flat] vertical, and rounded) at 0 and 2 α_p. The findings were:

- Rounded leading edges were superior to horizontally flat, which were superior to vertically flat.
- At 0.001 thickness, the performance varied little with leading edge shape; at 0.01 and greater the ***L/D*** were dependent on leading edge shape.
- A rounded leading edge was able to improve ***L/D*** for 0.01 and 0.02 thicknesses versus 0.001; however, other edge shapes showed decreasing ***L/D*** with increasing thickness.
- The most effective rounded leading edge is a NACA-type leading edge expressed over a narrow thickness and symmetric to the camber centerline as summarized by Equation 3.

The change in efficiency from 36 (Figure 7) to 67.5 ***L/D*** (Table 1) is likely due to the leading edge being effective for inducing thrust. When drag is already relatively low, small increases in induced thrust have a significant impact on ***L/D***.

Influence of α_P>1°

Figure 14 summarizes how thicker airfoils lead to larger pressure bubbles with higher pressures at the leading edge. The default contributor of this leading-edge pressure is increased drag. Airfoil shape and operating conditions can induce lower pressures on upper surface and transfer the leading-edge pressure bubble to more-horizontal lower surfaces of the airfoil, the entire body is transformed to a highly efficient lifting-body surface. Understanding this phenomenon could be key to designing aircraft with both thick fuselages and higher ***L/D*** (e.g., ***L/D*** > 30). This topic is a part of continuing research on generating high ***L/D*** low ***AR*** aircraft.

Sources of Lift Pressures

Ultimately, a lifting body mechanism needs sources of lift pressures, example sources include:

a) Free stream velocity impacting a lower surface,

b) Formation of a leading-edge low pressures due to leading edge pressure bubbles—caused by impacting velocities—which can a) expand upward ultimately cause air to diverge from surfaces above the leading edge and b) migrate to downward on the leading-edge surface,

c) a curvature of a surfaces causing air to impact or diverge from that surface,

d) a flap or other sudden change in wetted surface curvature, and

e) a propulsion source ("Source").

The lift pressures generated by these sources will expand at the speed of sound and will influence streamlines near the airfoil's surface. Use of distributed Sources to generate lift is a burgeoning area of aerodynamics outside the scope of the current work.

Lift Coefficients

Both drag coefficients and lift coefficients are strong functions of the camber as illustrated by Fig. 15 and Table 1. Higher α_A typically increase the lift coefficient. The impact of pitch angle on ***L/D*** depends can be highly dependent on the extent to which induced thrust cancels form drag making the impact of pitch angle less definitive. The impact of velocity in the range of 9 to 90 m/s for a 1m chord airfoil was less than 10% on ***L/D***, and the impact on lift coefficients was within the error of the data. Lift coefficients tend to increase with increasing frontal projected areas.

The ***L/D*** of preliminary 3D CFD simulations at low ***AR*** are summarized by Fig. 16. The loss of lift pressures over side edges dominates the ***L/D*** with values less than 20% of the airfoil ***L/D*** values at ***AR*** of 0.4 and 1.0. The

impact is less with higher camber thin-plate airfoils since ***L/D*** is a dynamic phenomenon where increased generated lift at higher α_P can compensate for lost lift.

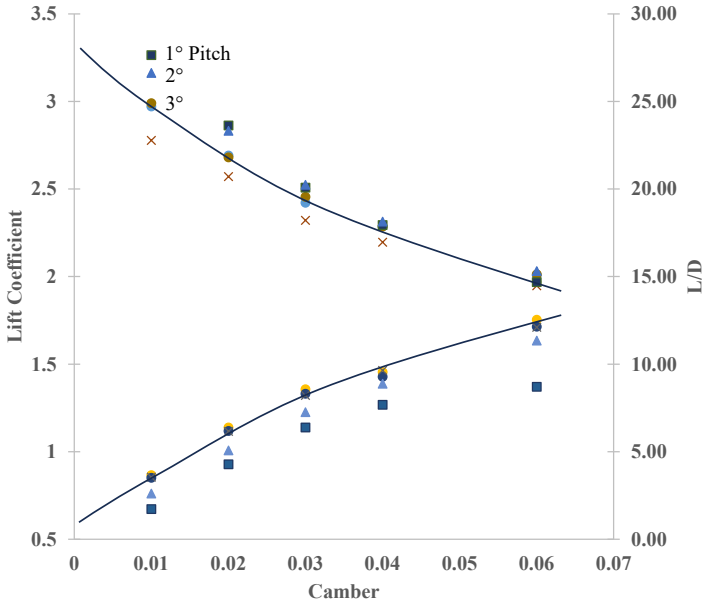

Fig. 15. Performances of thin-plate cambered airfoils. Vertical-cut and horizontal-cut leading edges are indistinguishable. All data are at 90 m/s free stream velocity except "X" at 9 m/s.

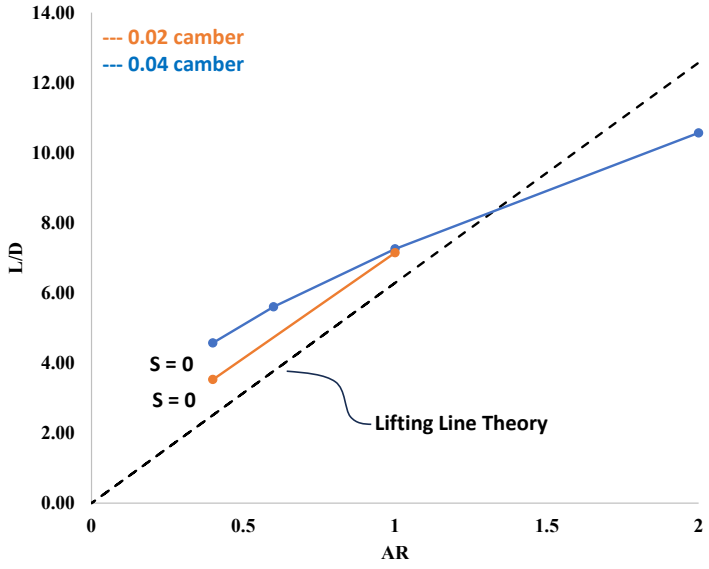

Fig. 16. Comparison of thin-plate cambered airfoil performance to lifting line theory at low aspect ratios.

Lower lift coefficients cause lower ***L/D***. Equation 4 relates wing loadings to lift coefficients. Wing loadings range from over 800 kg/m^2 for airliners to 4 kg/m^2 for 24/7 HAPS/HALE aircraft. And while C_L around 1.8 are

typical for airliners at cruising configurations, values of 0.2 are feasible with ultralight aircraft designs. Most of the previous works on thin cambered airfoils emphasized higher cambers (e.g., like 0.06), since higher lift coefficients are typically needed. For solar aircraft, lift coefficients as low as 0.02 are viable for cruising.

$$gW_S \frac{A}{2} = 0.5\,\rho U^2 A C_L \tag{4}$$

Table 2 summarizes heuristics that provide a starting point for designing optimal configurations for solar aircraft. These heuristics summarize many of the key points of this paper. As a list of heuristics, they provide a design tool and a list that can be continuously improved as more is understood on these topics.

Fig. 17 illustrates high surface area designs being considered for solar aircraft applications. [24, 25] The aircraft are a scalable version blended-body-wing (BWB) designs using; they use large sections of thin cambered wings including a center thin wing section. The aircraft illustrate distributed propulsion and fences along the thin center wing; two approaches on which work is continuing toward improving ***L/D*** and C_L for thin cambered wings.

Thin cambered wings lack the internal structures that are able to transfer loads from wider wingspans. The low ***AR*** thin central wings of the Fig. 17 architectures transfer minimal loads spanwise.

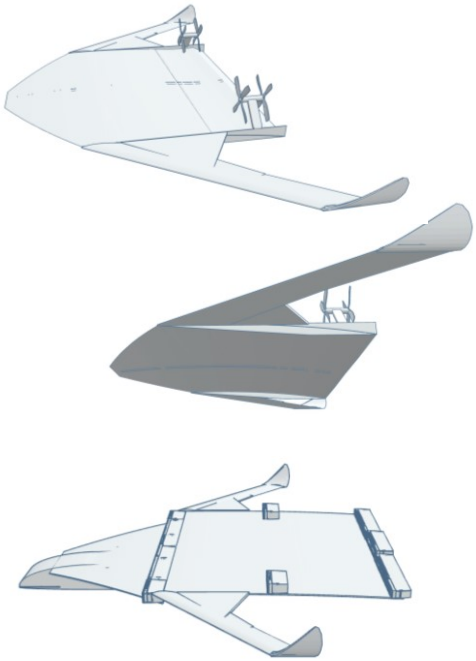

Fig. 17. Illustration of modified BWB design that uses large sections of thin-plate cambered wings.

Table 2. Heuristics on designing to create aerodynamic lift and flight efficiency.

For Airfoils (2D cross-sections):

- **A-1.** Air's velocity impacting a surface generates higher Pressure.
- **A-2.** Air's velocity diverging from a surface generates lower Pressure.
- **A-3.** Air expands at speed of sound from high-to-low Pressure (except within boundary layer).
- **A-4.** Air's velocity bends toward lower Pressure and away from higher Pressure.
- **A-5.** A surface's ***L/D*** is the normalized surface integral of Pressure $\tan^{-1}(\alpha)$ on the surface, per:

$$Lift = \Delta P\, \Delta S\, Cos(\alpha_P); \quad Drag_{form} = \Delta P\, \Delta S\, Sin(\alpha_P);$$
$$L/D = \frac{1}{Tan(\alpha_P)} = \frac{57}{\alpha_P^\circ} \; at\ low\ \alpha_P \qquad (1)$$

- **A-6.** Shear forces are negligible at $C_d > 0.01$; $C_{d,\,shear} < 0.001$ for smooth surface.

For the addition of Sources (Propulsion, i.e. jets, propellers, etc.):

- **S-1.** Increasing Source power increases Lift at trailing edge of Lift Spans; when Lift Span pitch angle < 0° from horizontal, Source power increases ***L/D*** as limited by Operating Point.
- **S-2.** For ***L/D*** > 40, induced thrust is necessary; induced thrust counteracts Drag.
- **S-3.** For the highest ***L/D***: the Lift Span, Nose, and (optional) wings need to have pitches coordinated with Lift Span interaction with a Source.
- **S-4.** High induced Drag on surfaces > 3° should be eliminated by transforming pressure to near free stream pressures or transforming surface through addition of induced thrust.
- **S-5.** A mid-chord Source can propagate lower pressure forward to increase overall ***L/D***.
- **S-6.** Optimal Lift Span pitches decrease with increasing Source power.

For Wings (i.e. 3D airfoils):

- **W-1.** Lift pressures are lost over side edges for a wing relative to an airfoil.
- **W-2.** Use camber, fences, and distributed Sources to compensate for lost Lift pressure.
- **W-3.** High ***AR*** wings may be added to low ***AR*** lifting bodies to increase ***L/D***.
- **W-4.** Wing loadings vary with application, approximately: Military jets (700 kg/m^2, with C_L of 1.5), commercial jets (300-500, 1.5-1.6), commercial prop aircraft (100-200, 0.8), prop drones (50, 0.5)C, and HAPS/HALE (2-7, <0.4). When essentially all the planform generates lift, $C_L = [m\ g] / [\rho\ A\ u^2]$. Where at a planform loading 2, $C_L = 2\ g / [\rho\ u^2]$. At 80 m/s and 0.1 kg/m^3 $C_L = 0.03$ (i.e., HAPS aircraft have much lower C_L than jets).

Conclusions

Design methods described in this paper can be reliably used to create high ***L/D*** for thin-plate cambered airfoils. However, 2D airfoil ***L/D*** and C_L do not quantifiably translate to performance of 3D thin-plate cambered wings due to air flow over side edges. A set of heuristics have been compiled to summarize guidelines, trends, and benchmark values for designing airfoils; they provide a starting point for wing and airframe designs using thin-plate wing sections.

While side-edge losses are detrimental to performance on airliners and military jets, the low wing loadings of many solar aircraft designs enable compatibility with lower ***L/D*** wing sections. Bifacial solar plates configured as thin cambered wings create higher specific solar productivity (e.g., W/kg) and relax ***L/D*** requirements. Also, novel scalable BWB designs using thin central wings, fences, and distributed propulsion have additional degrees of freedom to overcome side-edge losses.

References

[1] Deline, C., Palaez, S.A., Marion, B., "Bifacial PV System Performance: Separating Fact from Fiction," [online database]https://www.nrel.gov/docs/fy19osti/74090.pdf [cited Nov 27, 2023].

[2] "Albedo," 2023, see https://en.wikipedia.org/wiki/Albedo .

[3] "Bifacial solar photovoltaics – A technology review - ScienceDirect,"

[4] Burgmann, S. Dannemann, J. & Schroder, W., "Time-resolved and volumetric PIV measurements of a transitional separation bubble on an SD7003 airfoil | SpringerLink," *Experiments in Fluids,* Vol. 44, 2007, pp. 609-622.

[5] Klose, B., Spedding, G., and Jacobs, G., "Direct numerical simulation of cambered airfoil aerodynamics at Re = 20,000," 2021,

[6] Michna, J., and Rogowski, K., "Numerical Study of the Effect of the Reynolds Number and the Turbulence Intensity on the Performance of the NACA 0018 Airfoil at the Low Reynolds Number Regime," *Processes,* Vol. 10, 2022, pp. 1004.

[7] Mirhashemi, A., Chapman, J.W., Miller, C.J., "Tail-mounted engine Architecture and Design for the Subsonic Single Aft Engine Electrofan Aircraft," San Diego, CA,

[8] Jansen, R.H., Kiris, C.C., Chau, T., "Subsonic Single Aft Engine (SUSAN) Transport Aircraft Concept and Trade Space Exploration," San Diego, California,

[9] Russo, O., "Computational Fluid Dynamics analyses of a wing with distributed electric propulsion," 2022,

[10] Serrano, J., Tiseira, A., García-Cuevas, L., "Computational Study of the Propeller Position Effects in Wing-Mounted, Distributed Electric Propulsion with Boundary Layer Ingestion in a 25 kg Remotely Piloted Aircraft," *Drones,* Vol. 5, 2021, pp. 56.

[11] Osei, Emmanuel Yeboah, Opoku, Richard, Sunnu, Albert K. Adaramola, Muyiwa S., "Development of High Performance Airfoils for Application in Small Wind Turbine Power Generation," *Journal of Energy,* Vol. 2020, 2020,

[12] Lee, D., Nonomura, T., Oyama, A., "Comparison of Numerical Methods Evaluating Airfoil Aerodynamic Characteristics at Low Reynolds Number," *Journal of Aircraft,* Vol. 52, 2015, pp. 296-306.

[13] Achour, G., Sung, W., Pinon, O., "Development of a Conditional Generative Adversarial Network for Airfoil Shape Optimization," 2020-01-06,

[14] Wu, R., Soutis, C., Zhong, S., "A morphing aerofoil with highly controllable aerodynamic performance," *The Aeronautical Journal,* Vol. 121, 2016, pp. 1-19.

[15] Felder, J., Brown, G., DaeKim, H., "Turboelectric Distributed Propulsion in a Hybrid Wing Body Aircraft," 12 September 2011,

[16] Kim, H.D., and Perry, AT, Ansell, PJ, "A Review of Distributed Electric Propulsion Concepts for Air Vehicle Technology," 2018.

[17] Gohardani, A., Doulgeris, G., and Singh, R., "Challenges of future aircraft propulsion: A review of distributed propulsion technology and its potential application for the all electric commercial aircraft," *Progress in Aerospace Sciences,* Vol. 47, 2011, pp. 369-391.

[18] McDonald, R.A., German, B.J., Takahashi, T., "Future aircraft concepts and design methods," *The Aeronautical Journal,* Vol. 126, No. 1295, 2022, pp. 92-124.

[19] Anonymous "Patent Portfolio," [online database]http://www.terretrans.com/tech.html [cited Jul 31, 2023].

[20] Finger, D., Braun, C., and Bil, C., "A review of configuration design for distributed propulsion transitioning VTOL aircraft," 2017,

[21] Borer, N.K., Derlaga, J.M., Deere, K.A., "Comparison of Aero-Propulsive Performance Predictions for Distributed Propulsion Configurations," Grapevine, TX, January 9, 2017,

[22] Erhard, R., Clarke, M., and Alonso, J., "A Low-Cost Aero-Propulsive Analysis of Distributed Electric Propulsion Aircraft," January 11, 2021,

[23] "NACA airfoil," 2023, (see https://en.wikipedia.org/wiki/NACA_airfoil).

[24] Suppes, A., and Suppes, G., "Highly-Efficient Low-AR aerial vehicles in urban transit," *Proceedings of the 2014 Transportation Research Board Annual Meeting,* January, 2024, (see preprint http://www.terretrans.com/opensource.html).

[25] Suppes, A., and Suppes, G., "Thermodynamic Analysis of Distributed Propulsion," *Cnet,* Submitted for Review (preprint available), (see preprint http://www.terretrans.com/opensource.html) .